Applied Physics A (2019) 125:705
https://doi.org/10.1007/s00339-019-3000-3

Applied Physics A
Materials Science & Processing

The electronic and optical properties of an exciton, biexciton and charged excitons in CdSe/CdTe-based multi-shell type-II quantum dot nanocrystals

Fatih Koç[1,2] · **Mehmet Sahin**[3]

Received: 22 April 2019 / Accepted: 6 September 2019 / Published online: 17 September 2019

Abstract
It has been recently reported that multi-shell type-II quantum dot nanocrystals (QDNCs) have higher quantum yields. Besides these higher quantum yields of multi-shell type-II QDNCs, additional second layer has been a critical influence on the formation mechanisms of the excitonic structures. Understanding of bound and unbound cases of the excitonic structures in multi-shell type-II QDNCs gives some important information for applications. In this study, we have investigated the electronic and optical properties of a single exciton (X), biexciton (XX), and positively and negatively charged excitons (X^+ and X^-) in CdSe/CdTe-based multi-shell type-II QDNCs. In the study, three different structure compositions, i.e., CdSe/CdTe, CdSe/CdTe/CdS, and CdSe/CdTe/ZnTe, have been considered. We have observed that CdS and ZnTe materials have drastically changed the electronic and optical properties of the bare CdSe/CdTe type-II QDNCs.

1 Introduction

The latest developments in crystal growth techniques has made possible to produce multi-shell quantum dot nanocrystals (QDNCs) with control of the electronic properties [1–4]. Quantum dot nanocrystals, because of this tunability of the electronic properties depending on their size and/or material, are unique candidates to fabricate of the quantum dot lasers [5–8], biological imaging devices [9–11], quantum dot light-emitting diodes (LED) [12–15], photovoltaic [16–22] and spintronics [24] applications. As well known, if both carriers (i.e., electron and hole) are confined into the same spatial region of a QDNC, this structure is called as a type-I QD heterostructure. On the other hand, if the carriers are confined in different spatial regions of a core/shell QDNC, this one is termed as type-II QDNC. The confinement type of QDNCs is dependent directly on their material properties. Each structure has different physical properties and superiorities for different device applications. For example, while type-I QDNCs are appropriate for LED devices, type-II QDNCs are proper for photovoltaic devices such as solar cells. On the other hand, multi-shell type-II QDNCs can bring a new perspective to type-II QDNCs for the LED applications [25].

In type-II structures, while the energy levels of the electron and hole can be tuned separately by adjusting the core size or shell thickness [27–30], this kind of controlling is not possible in type-I heterostructures [31]. Therefore, this controllability of the electronic structures of type-II QDNCs has distinct superiority when compared to that of type-I counterparts. Similarly, the exciton lifetime can also be tuned much more effectively in type-II QDNC heterostructures [32]. In addition, when the core and shell materials are replaced with each other, confinement regions of the electron and hole replace by one another and so the electronic and optical properties can largely become different. As well as many advantages of type-II QDNCs, these structures have a bad reputation owing to their low quantum yields at the same time. But it seems that multi-shell type-II QDNCs can be overcome this bad reputation thanks to their high quantum yields [25, 31, 33].

✉ Mehmet Sahin
mehmet.sahin@agu.edu.tr; mehsahin@gmail.com

Fatih Koç
fatih.koc@msn.com

[1] Department of Physics, Faculty of Sciences, Selcuk University, 42075 Konya, Turkey

[2] Department of Vocational School of Health Services, Igdir University, Igdir, Turkey

[3] Department of Materials Science and Nanotechnology Engineering, School of Engineering, Abdullah Gül University, Sümer Campus, 38080 Kayseri, Turkey

The type-II structures are the subject of a great interest both theoretically [29, 30, 34–36] and experimentally [19, 27, 31, 37–50] due to these outstanding properties. Especially, CdSe/CdTe type-II QDs are very promising structures for photovoltaic applications and there are some studies related to these structures in the literature [20, 52]. Leontiadou et al. [52] investigated effect of the shell thickness on the efficiency of CdSe/CdTe QD solar cells. In addition, they examined the exciton lifetime as a function of shell thickness in the same structures.

Although there are a number of experimental studies reported on the excitons in type-II QDNCs in the literature as well as theoretical ones, the studies on charged excitons and biexcitons in the type-II QDNCs are still unsatisfying. Understanding in details of charged excitons and biexcitons in the type-II QDNCs is crucial for device fabrication, especially photovoltaic devices. For example, the electronic structure of a type-II core/shell QDNC can be substantially changed when an additional second layer covers onto the shell layer of the QDNC.

In our previous study, we investigated the effect of a buffer layer on the electronic and optical properties of an X and XX in type-II CdTe/CdSe QDNCs. As mentioned above, the electronic properties of a type-II QDNC can be substantially changed when the core and shell materials are switched their places. Therefore, in this work, we consider CdSe/CdTe QDNC and its derivatives. In this context, the primary goal of this study is to investigate the electronic and optical properties of exciton (X), biexciton (XX) and positively and negatively charged excitons (X^+ and X^-) in type-II CdSe/CdTe, CdSe/CdTe/CdS, and CdSe/CdTe/ZnTe QDNCs. To determine the electronic properties of the considered structures, i.e., energy levels and corresponding wavefunctions, the Poisson–Schrödinger equations have been solved self-consistently in the Hartree approximation. Using these energy levels and wavefunctions, the optical properties, such as overlap integral, absorption wavelength, oscillator strength, lifetime, of the X, XX, X^+ and X^- in type-II CdSe/CdTe have been carried out for cases with and without different second layer materials, CdS and ZnTe. The obtained results and their possible physical reasons have been discussed in a detail manner.

2 Model and theory

We have considered a spherically symmetric type-II CdSe/CdTe/organic coating (i.e., core/shell/ligand) QDNC and its derivatives in which a second shell is covered between shell and ligand, i.e., CdSe/CdTe/CdS/ligand and CdSe/CdTe/ZnTe/ligand. The potential profile of CdSe/CdTe/CdS and CdSe/CdTe/ZnTe structures are demonstrated in Fig. 1.

In frame of the envelope function effective mass approximation and BenDaniel–Duke boundary condition [26], single-particle Schrödinger equations for multi excitons can be written as:

$$\left[-\frac{\hbar^2}{2}\vec{\nabla}_r\left(\frac{1}{m_e^*(r)}\vec{\nabla}_r\right) + V_e(r) - q_e\phi_h + q_e\phi_e + V_{xc}^{e-e}[\rho_e(r)]\right] R_e^s(r) = \varepsilon_e R_e^s(r), \tag{1}$$

and

$$\left[-\frac{\hbar^2}{2}\vec{\nabla}_r\left(\frac{1}{m_h^*(r)}\vec{\nabla}_r\right) + V_h(r) - q_h\phi_e + q_h\phi_h + V_{xc}^{h-h}[\rho_h(r)]\right] R_h^s(r) = \varepsilon_h R_h^s(r), \tag{2}$$

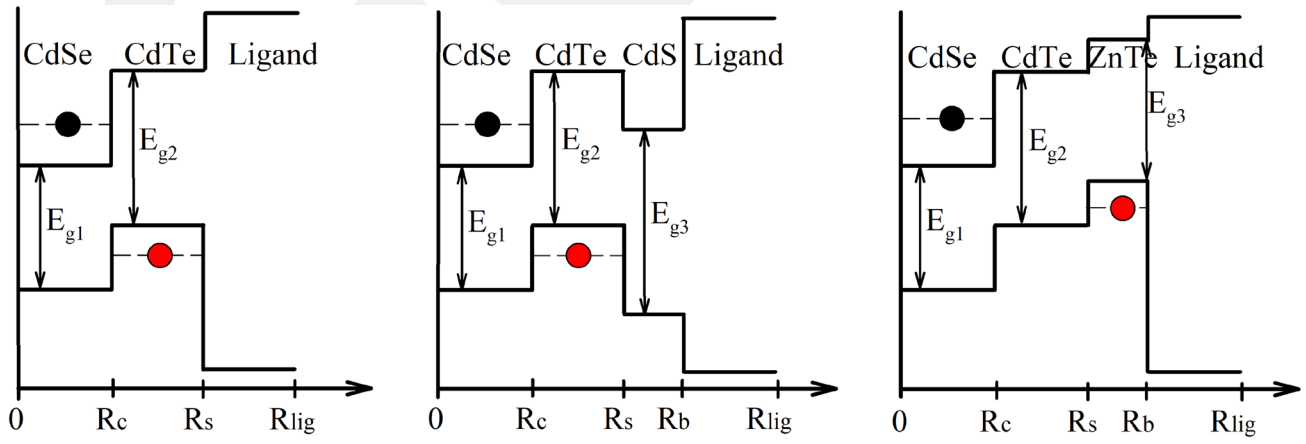

Fig. 1 Schematic representation of the potential profiles of the considered type-II structures for bare CdSe/CdTe QDNC (left panel), CdSe/CdTe/CdS QDNC (middle panel), and CdSe/CdTe/ZnTe QDNC (right panel). Black and red circles show the electrons and holes, respectively. Dashed lines demonstrate the single-particle energy levels of the electrons and holes

where $\hbar$ is the reduced Planck's constant, $m_e^*(r)$ and $m_h^*(r)$ are the position-dependent electron and hole effective masses, respectively, $V_e(r)$ and $V_h(r)$ are the electron and hole confinement potentials, respectively, q_e is the electron and q_h is the hole charges. The ϕ_e and ϕ_h are the electrostatic Coulomb potential due to the electron and hole, respectively. The $q_{e(h)}\phi_{h(e)}$ is the attractive Coulomb potential between the opposite charges and the $q_{e(h)}\phi_{e(h)}$ is the repulsive Coulomb potential between the same kinds of particles. The $V_{\rm xc}[\rho(r)]$ terms are the exchange-correlation (XC) potentials between the same signed particles, ε_e is single-particle energy eigenvalue of the electron and similarly, ε_h is single-particle hole energy, and $R_e^s(r)$ and $R_h^s(r)$ are the s-type radial wave functions of these energy states, respectively. It is noted that, in single-exciton cases, the repulsive Coulomb and XC potential terms are not taken into consideration.

These two equations are coupled with each other through the attractive Coulomb terms, $q_e\phi_h$ and $q_h\phi_e$. To find the single-particle energy levels of electron and hole, Eqs. (1) and (2) are solved self-consistently and simultaneously. On the other hand, if the QDNC contains more than one same kind of particle, in this case, the repulsive potentials between of them are computed self-consistently. Hence, all Coulomb effects on the energy eigenvalues and corresponding wave functions have been taken into account. The Coulomb potentials are calculated by solving of the Poisson equations:

$$\begin{aligned}\vec{\nabla}\kappa(r)\vec{\nabla}\phi_e &= \frac{q_e}{\varepsilon_0}\rho_e(r),\\ \vec{\nabla}\kappa(r)\vec{\nabla}\phi_h &= -\frac{q_h}{\varepsilon_0}\rho_h(r),\end{aligned} \tag{3}$$

where ρ_e is electron and ρ_h is hole densities [53], ε_0 is dielectric permittivity of the vacuum and $\kappa(r)$ is the position-dependent dielectric constant of the structure. These equations contain the image potential contributions originated from difference dielectric values of core and shell materials.

In calculation of the XC potential between the same particles, i.e., charged excitons and biexciton cases, Perdew-Zunger [54] expression, which is a parametrization of the Monte Carlo results of Ceperley and Alder [55], is employed. This expression of the XC potential contains the self-interaction corrections. In the case of strong confinement regime, it has been reported that electron–hole correlation energy can be negligible level relative to the electron–hole Coulomb energy [23]. Therefore, this energy term has not been included in our calculations.

To determine the electronic structure of the considered system, the last three equations, Eqs.(1), (2), and (3), must be computed self-consistently. For this purpose, in the real space formalism, the full numeric matrix diagonalization technique can be used. All details of the computation steps can be found in Ref. [29].

The binding energy of the X^+, X^- and XX can be calculated by means of [56]

$$\begin{aligned}E_b^{\mathsf{X}^+} &= E_{\mathsf{X}}^{\rm tot} + \varepsilon_h^{(0)} - E_{\mathsf{X}^+}^{\rm tot},\\ E_b^{\mathsf{X}^-} &= E_{\mathsf{X}}^{\rm tot} + \varepsilon_e^{(0)} - E_{\mathsf{X}^-}^{\rm tot},\\ E_b^{\mathsf{XX}} &= E_{\mathsf{XX}}^{\rm tot} - 2E_{\mathsf{X}}^{\rm tot},\end{aligned} \tag{4}$$

where $\varepsilon_{e,h}^{(0)}$ is isolated single electron (hole) energy in the structures. $E_{\mathsf{X}}^{\rm tot}$ is the single exciton, $E_{\mathsf{X}^+}^{\rm tot}$ is the positively and $E_{\mathsf{X}^-}^{\rm tot}$ is the negatively charged excitons and $E_{\mathsf{XX}}^{\rm tot}$ is the biexciton total energies and these energies discussed in detail in our previous work [51].

The oscillator strength, a measure of the optical transitions, is crucial parameter in studying of all optical properties of any quantum structures from atoms to solids. The single-exciton oscillator strength is given as [57]:

$$f_{\mathsf{X}} = \frac{E_p}{2E_{\mathsf{X}}}\left|\int r^2 {\rm d}r R_e^s(r)R_h^s(r)\right|^2, \tag{5}$$

where E_p is the Kane energy, E_{X} is the exciton transition energy, $R_e(r)$ and $R_h(r)$ are the radial part of electron and hole wavefunctions, respectively.

The recombination oscillator strengths of the X^+, X^- or XX are calculated by means of

$$f_{\mathsf{X}^+,\mathsf{X}^- or \mathsf{XX}} = A\frac{E_p}{2E_{\mathsf{X}^+,\mathsf{X}^- or \mathsf{XX}}}\left|\int r^2 dr R_e(r)R_h(r)\right|^2, \tag{6}$$

where $E_{\mathsf{X}^+,\mathsf{X}^- or \mathsf{XX}}$ is the transition energy of the considered system (X^+, X^- or XX), and $R_e(r)$ and $R_h(r)$ are the corresponding radial wavefunction of the electron and hole. Here, A is a recombination probability of the system and the factor $A \simeq 2$ for the bound and $A = 1$ for the unbound X^+ and X^-. On the other hand, the factor $A \simeq 4$ for the bound and $A \simeq 2$ for the unbound XX. The details of this approximation can be found in Ref. [28].

The radiative lifetime is another important quantity in both theoretical and experimental investigation of the excitonic structures [27, 58–60]. The mathematical expression of the radiative lifetime is given as [61, 62]:

$$\tau = \frac{6\pi\varepsilon_0 m_0 c^3\hbar^2}{e^2 n\beta_s E^2 f}, \tag{7}$$

where ε_0 is the dielectric permittivity of the vacuum, m_0 is the free electron mass, c is the light velocity in the vacuum, e is the bare electronic charge, f is the oscillator strength, n is the refractive index of QDNC material, E is the transition energy of considered system and β_s is the screening factor [62].

3 Results and discussion

The atomic units are used throughout the calculations. In this units, the Planck constant, $\hbar$, bare electron mass m_0, and fundamental electronic charge e are equal to unity. All material parameters used in the calculations are listed in Table 1. The effective exciton Bohr radius and the effective Rydberg energy are $a_0 = 71.06$ Å and $R_y = 9.74$ meV, respectively, in terms of the CdSe material parameters. In all structures, the core radius has been set to $R_c = 1.95$ nm.

The potential profile of the considered structures are shown in Fig. 1. In these structures, CdS and ZnTe are chosen as the second shell layers and thicknesses of them are fixed to 0.1 a_0 in the calculations. In left panel of the figure, while the electron(s) are substantially confined into the CdSe core region, hole(s) are confined into the CdTe shell of CdSe/CdTe QDNC. In middle panel of the figure, it is seen that a third material, i.e., CdS, is grown between shell and ligand as if a buffer layer. In right panel of the figure, the CdS layer is replaced by ZnTe. Thereby, the potential profile is modified and it is expected that the modification, in middle panel, will be effective especially on the energy level of electron(s) while the modification in right panel will especially affect the energy level of the hole(s).

The position-dependent effective masses and dielectric constants are given as:

$$m^*_{e,h}(r) = \begin{cases} m^*_{e,h}(\text{CdSe}), & r \le R_C \\ m^*_{e,h}(\text{CdTe}), & R_C < r \le R_S \\ m^*_{e,h}(\text{buff}), & R_S < r \le R_B \\ m^*_{e,h}(\text{lig}), & r > R_B \end{cases}, \qquad \kappa(r) = \begin{cases} \kappa(\text{CdSe}), & r \le R_C \\ \kappa(\text{CdTe}), & R_C < r \le R_S \\ \kappa(\text{buff}), & R_S < r \le R_B \\ \kappa(\text{lig}), & r > R_B \end{cases}. \tag{8}$$

Figure 2 depicts changes of the total energies of the X, XX, X^+, and X^- in CdSe/CdTe, CdSe/CdTe/CdS, CdSe/CdTe/ZnTe QDNCs as a function of the CdTe shell thickness. The total energies of all structures, as expected, decrease with increasing shell thickness and this decreasing is more distinctly in CdSe/CdTe and CdSe/CdTe/CdS QDNCs while it is not so dramatic in CdSe/CdTe/ZnTe QDNC. When we look at the potential profile, we conclude that, in the first and second structures, changing of the shell region affects directly the energy level of the hole(s) since the hole(s) are confined into the CdTe shell. Therefore, the total energy changing interval with respect to shell thickness is the most in CdSe/CdTe structures for all exciton complexes. However, although it is not very obvious, the electron(s) energy levels are affected from changing of the shell region thickness depending on the penetration of the electron wave functions into the shell region. In the third structure, right panel of Fig. 1, confinement of the hole(s) will most probably be inside the ZnTe shell depending on the CdTe shell thickness. For that reason, neither electron(s) nor hole(s) energy states are affected drastically from changing of the shell thickness. On the other hand, the attractive Coulomb interaction will decrease with increasing shell thicknesses.

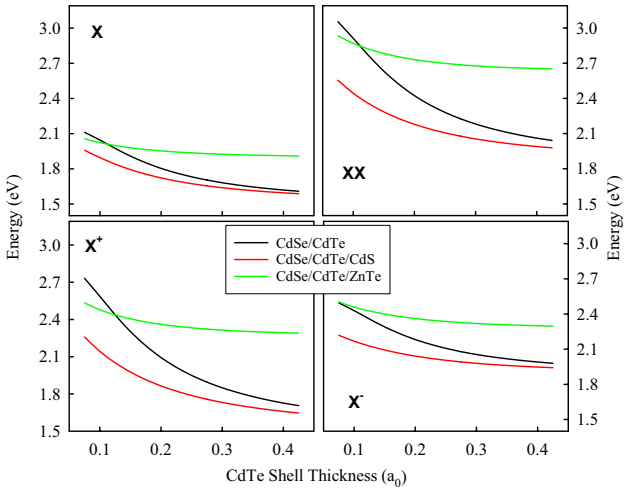

Fig. 2 Total energy of the X, XX (top panel) and X^+, X^- (bottom panel) as a function of the CdTe shell thicknesses for three different QDNC structures

Binding energies of excitonic structures are other important quantities. Origin of the binding energy is the attractive Coulomb potential between the electron(s) and hole(s). If a single exciton is unbound, the electron and hole move

Table 1 The material parameters used in the calculations

Material	m^*_e/m_0	m^*_h/m_0	κ	E_g	$V_e(eV)$	$V_h(eV)$
CdSe	0.12 [35]	0.45 [35]	9.29 [63]	1.76 [64]	(CdTe–CdS) 0.10 [64]	(CdTe–CdS) 0.99 [64]
CdTe	0.096 [35]	0.4 [35]	10.4 [63]	1.61 [64]	(CdTe–CdSe) 0.42 [64]	(CdTe–CdSe) 0.57 [64]
CdS	0.2 [63]	0.7 [63]	8.73 [63]	2.50 [64]	(CdTe–ZnTe) 1.10 [65]	(CdTe–ZnTe) 0.40 [65]
ZnTe	0.122 [63]	0.6 [63]	10.3 [63]	2.26 [65]	(CdS–ligand) 2.75	(CdS–ligand) 2.75
Ligand	1.0 [35]	1.0 [35]	2.0 [35]	8.0 [35]	(ZnTe–ligand) 2.87	(ZnTe–ligand) 2.87

independently from each other and hence, these carriers can be separated relatively easily and in this case, there is no an exciton in exact manner. Actually, there is just an electron–hole pair. However, in semiconductor quantum nanostructures, especially in quantum dots, single excitons are in bound forms. As for trions, bound trion term corresponds to a situation in which all particles behave as a single particle. Namely, the attractive Coulomb potential is more dominant than repulsive interactions between the same charges. In case of an unbound trion, the repulsive Coulomb potential is dominant and this structure is dealt as an exciton and an excess charge, that is an electron in X^- and a hole in X^+. Similarly, in an XX structure, if the attractive Coulomb potential between the electrons and holes is higher, all of the charges move as a single particle and are called as a bound biexciton. In an unbound biexciton case, the repulsive Coulomb potential is stronger and this structure can be considered as two independent excitons [28]. The unbound excitonic structures are more proper for photovoltaic applications when compared to the bound excitons. Conversely, bound excitonic structures, observed especially in type-I QDNC, are more appropriate for illumination devices such as, LED. Figure 3 demonstrates the binding energies of the X, XX, X^+, and X^- in CdSe/CdTe, CdSe/CdTe/CdS, and CdSe/CdTe/ZnTe QDNCs as a function of the CdTe shell thicknesses. When we look at the binding energy of the X, we see that the changing of it in CdSe/CdTe exhibits a typical exciton-binding energy behavior. That is, it decreases with increasing shell thickness. And also the highest exciton binding energy value is observed again in this QDNC. This can be explained as follows: in smaller shell thicknesses, the hole pushes towards the core region and so the attractive Coulomb interaction becomes higher due to smaller

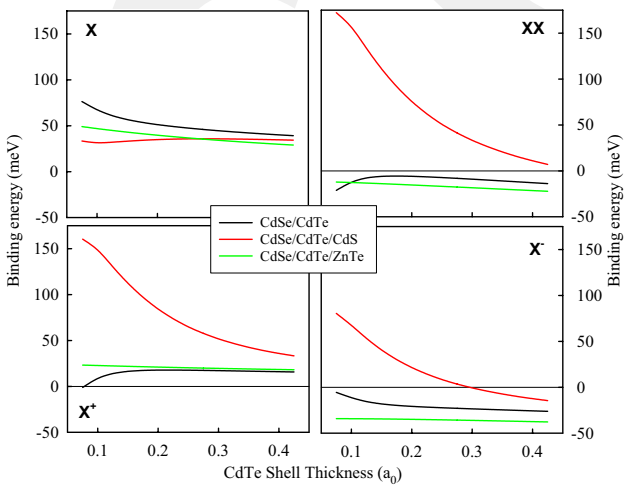

Fig. 3 Binding energy of the X, XX (top panel) and X^+, X^- (bottom panel) as a function of the CdTe shell thicknesses for three different QDNC structures

distance between the electron and hole and with increasing shell thickness this attractive Coulomb energy becomes smaller because of the larger distance between the electron and hole. Yet, in other two QDNCs with CdS and ZnTe additional shells, the binding energy values are smaller and especially in CdSe/CdTe/CdS QDNC, the binding energy value is almost unchanging with increasing shell thickness. This is because the probability distribution of the electron expands to whole structure and hence, the Coulomb interaction becomes approximately constant. In CdSe/CdTe/ZnTe QDNC, since the hole is substantially confined into the ZnTe shell, the attractive Coulomb interaction is decreasing with increasing shell thickness for the exciton. When we look at the XX panel, we see that this structure is unbound in bare CdSe/CdTe QDNC and its derivative with ZnTe layer. Its reason is that the repulsive Coulomb interaction between the charges with the same sign is predominant when compared to the attractive Coulomb interactions between the electrons and holes. On the other hand, in CdSe/CdTe/CdS QDNC, the attractive Coulomb interaction is more dominant and so a bound XX structure emerges. This result is so crucial in terms of demonstrating that controlling of the binding situations of the XX depending on the second shell material. As for the X^+ and X^- structures, while positively charged exciton is bound in all three QDNCs (except shell thickness of 0.075 a_0 for CdSe/CdTe QDNC), negatively charged exciton is unbound in CdSe/CdTe and CdSe/CdTe/ZnTe QDNCs and it is bound until a certain value of the shell thickness in CdSe/CdTe/CdS QDNC. It can be concluded that, in the X^+, the attractive Coulomb interactions are larger. On the other hand, in the X^-, the repulsive Coulomb interactions are more dominant in case of unbound situations.

The absorption wavelength, which corresponds to the transition energy, is another important parameter of the QDNCs for device applications of these structures. Figure 4 shows the changes of the absorption wavelengths for the X and XX (top panel), and X^+ and X^- (bottom panel) as a function of the CdTe layer thickness. As seen from the figures, in all structures, the absorption wavelengths increase (red shift) with increasing of the shell thicknesses. This behavior is an expected situation since the energy levels are inverse proportional to the size of the quantum structures. Yet, the interesting situation for the exciton is while changing intervals are approximately between 575 and 780 nm in CdSe/CdTe and CdSe/CdTe/CdS QDNCs, this interval is very narrow, between 600 and 650 nm, in CdSe/CdTe/ZnTe QDNC. Similar observation in CdSe/CdTe QDNCs has been reported by Leontiadou et al. [52]. In their study, when the shell thickness is smaller than 0.5 nm, the structure exhibits quasi-type-II (or type-I) properties. In this study, the shell thickness starts almost from 0.5 nm, and, therefore, the quasi-type-II regime is not so apparent for the X structure. Another observation is that the absorption wavelength of

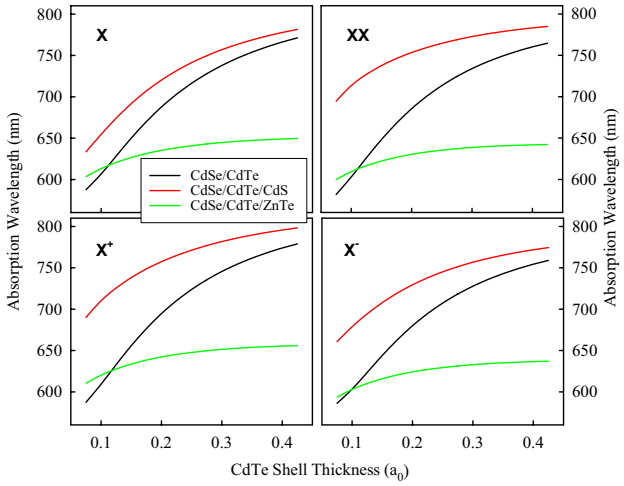

Fig. 4 Absorption wavelength of the X, XX (top panel) and X^+, X^- (bottom panel) as a function of the CdTe shell thicknesses for three different QDNC structures

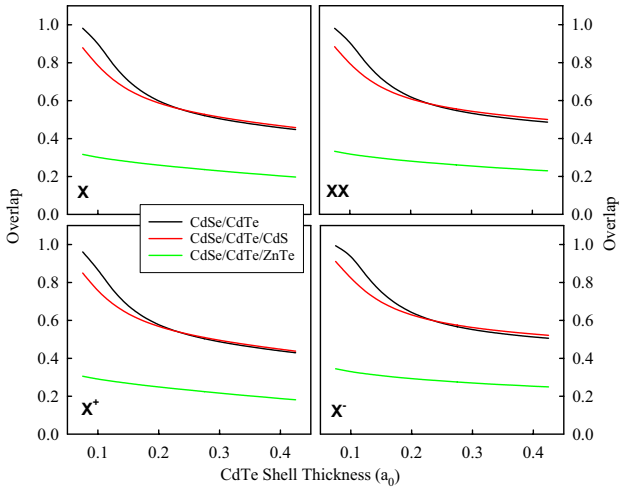

Fig. 5 Overlap integral of the X, XX (top panel) and X^+, X^- (bottom panel) as a function of the CdTe shell thicknesses for three different QDNC structures

the X is beginning from lower than 650 nm in CdSe/CdTe/CdS QDNC while the absorption wavelength of the other excitonic complexes starts from higher than 650 nm, it is almost 700 nm for X^+ and XX. Overall observation is that the absorption wavelengths are strongly dependent on the CdTe shell thickness in all QDNCs except for CdSe/CdTe/ZnTe QDNC. This is because the hole(s) are confined to the CdTe shell region in first two structures. On the other hand, in the third structure, the hole(s) are substantially confined into ZnTe layer and the thickness changing of the shell region does not affect dramatically the absorption wavelength of QDNC with the ZnTe shell.

The overlap integral is a unitless quantity and it is key in calculation of the oscillator strength. This important parameter gives an information about the overlapping of the electron and hole wavefunctions. Figure 5 demonstrates the overlap integral of all excitonic complexes in QDNCs. In overall glance, we see that the overlap integral of all X, XX, X^+, and X^- is approximately unity when the shell thickness is very small in CdSe/CdTe and CdSe/CdTe/CdS QDNCs and it decreases with increasing shell thicknesses. This is because when the shell thicknesses are smaller, the hole(s), due to the pushing to core region, are localized almost in the same spatial region with the electron(s). This localization of the hole wavefunction disappear with increasing shell thicknesses and consequently the overlap becomes weaker. Nevertheless, in CdSe/CdTe/ZnTe QDNC, the hole(s) are considerably confined into the ZnTe layer due to the lower potential and hence, the overlap of wavefunctions is already smaller and is not affected drastically from the changing of the shell thicknesses.

The oscillator strength is a dimensionless quantity and it can be considered as the probability of absorption or emission of light in optical transitions of a quantum mechanical system. Figure 6 shows the radiative recombination oscillator strengths (ROS) of the X, XX, X^+, and X^- as a function of the CdTe shell thickness. The ROS values of the X, XX, X^+, and X^- are minimum in QDNC with the ZnTe layer. This is because the overlap integrals of CdSe/CdTe/ZnTe QDNCs are smaller for all exciton structures. In CdSe/CdTe and CdSe/CdTe/CdS QDNCs, changing of the ROS of the X and X^+ are very similar to each other. When the shell thickness is very small (0.075 a_0), the ROS of X^+ in CdSe/CdTe QDNC becomes smaller because the X^+ is unbound at this thickness value. As known, if there are two exciton structures in a QDNC, they can form a biexciton (bound

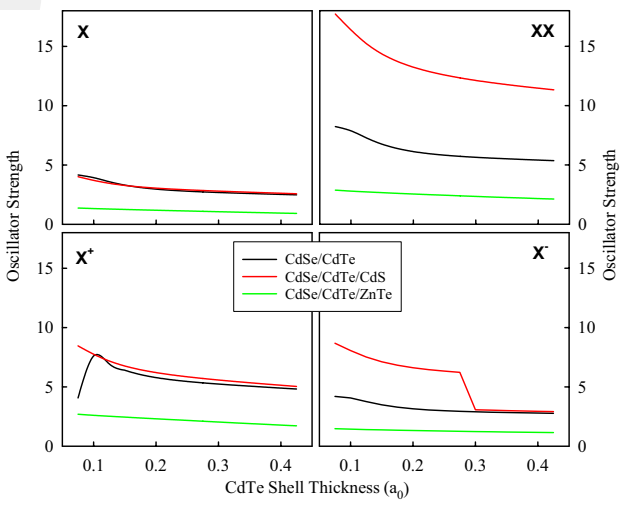

Fig. 6 Oscillator strength of the X, XX (top panel) and X^+, X^- (bottom panel) as a function of the CdTe shell thicknesses for three different QDNC structures

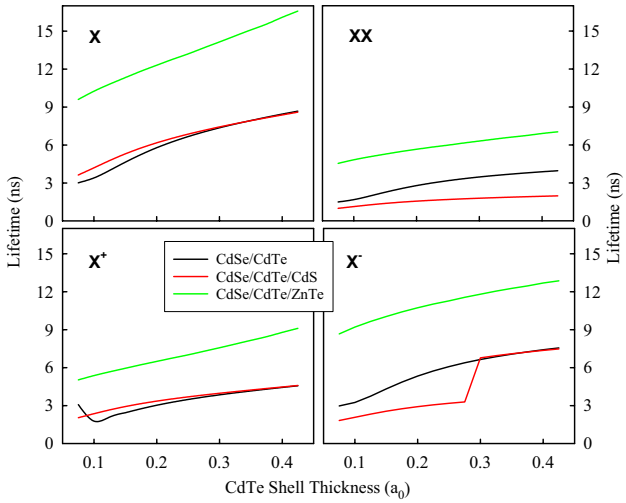

Fig. 7 Radiative lifetime of the X, XX (top panel) and X^+, X^- (bottom panel) as a function of the CdTe shell thicknesses for three different QDNC structures

structure) or two independent excitons, called unbound biexciton, depending on the interaction between X and X. Similar explanations can be done for X^+ and X^- structures. Hence, the factor *A* in Eq. (6) takes different values for the bound and unbound cases. In the unbound case of X^+ or X^-, as mentioned in model and theory section, the factor *A* is unity and it becomes two in the bound cases. Similarly, the factor A is two for the unbound biexciton cases while it is four for the bound biexcitons. Variations of the ROS of the XX and X^- are similar to each other until shell thickness is 0.3 a_0. At this thickness value, X^- in CdSe/CdTe/CdS QDNC is unbound and so the oscillator strength becomes smaller suddenly due to changing of the factor A.

In investigation of the potential device application of the QDNCs, the radiative lifetime of the excitons is extremely important and, therefore, in almost all experimental studies, the lifetime measurements have an extensive place. In Fig. 7, the radiative lifetimes of the X, XX, X^+, and X^- are plotted as a function of the CdTe shell thickness. As can be seen from the figure, the lifetimes range from 2 to 20 ns. It is clearly seen that all exciton complexes have the longest lifetime in the QDNC with the ZnTe additional shell. This is because the hole(s) are almost completely confined into the second shell. In other two QDNCs, CdTe/CdSe and CdTe/CdSe/CdS, the lifetime values are almost the same in a wide region, especially in the X and X^+ structures. On the other hand, an apparent separation is observed between the lifetime values of the XX and X^- structures, depending on whether they are bound or not. As can be seen from Eq.(7), the lifetime is proportional inversely with the oscillator strength and its values are different for the bound or unbound cases as explained in discussion of Fig.6. Therefore, these changes in the oscillator strength will affect directly the radiative lifetimes. Hence, the lifetime of the bound XX becomes shorter when compared to its unbound counterpart. Similar explanation is also valid for X^+ and X^- structures. In the literature, some experimental studies[66] related to the lifetime of biexcitons and trions, in which radiative lifetime of the XX and X^+ is explained using similar model we proposed, are available.

4 Conclusion

In this work, we have explored the electronic and optical properties of the X, XX, X^+, and X^- in CdSe/CdTe, CdSe/CdTe/CdS, and CdSe/CdTe/ZnTe QDNCs in a detail. To carry out the electronic structure calculations, the Poisson and Schrödinger equations have been solved self-consistently in the Hartree approximation for all structures. The optical properties, absorption wavelengths, overlap integrals, oscillator strengths, and radiative lifetimes have been determined using the obtained energy values and wavefunctions. We observe that all electronic and optical properties of the excitonic structures are strongly affected from potential profile and thickness of the additional second shell materials, CdS and ZnTe. This controllability provides a very important opportunity in terms of design of the type-II multi-shell QDNCs for some specific applications. It is hoped that this detailed investigation will give important informations to scientists in understanding of the X, XX, X^+, and X^- structures in multi-shell type-II QDNCs.

Acknowledgements This study was supported by TUBITAK TBAG with project number 109T729. One of the authors (MS) thanks Abdullah Gul University Foundation (AGUV) for their partial financial support.

References

1. D. Bimberg, M. Grundmann, N.N. Ledentsov, *Quantum dot heterostructures* (Wiley, Chichester, 1999)
2. V.I. Klimov, *Nanocrystal Quantum Dots*, 2nd edn. (CRC, Taylor and Francis Group, LLC, Boca Raton, 2010)
3. E.A. Dias, J.I. Saari, P. Tyagi, P. Kambhampati, Improving optical gain performance in semiconductor quantum dots via coupled quantum shells. J. Phys. Chem. C **116**, 5407–5413 (2012)
4. R.K. Ratnesh, M.S. Mehata, Synthesis and optical properties of core-multi-shell CdSe/CdS/ZnS quantum dots: surface modifications. Opt. Mater. **64**, 250–256 (2017)
5. N. Kirstaedter, O.G. Schmidt, N.N. Ledentsov, D. Bimberg, Gain and differential gain of single layer InAs/GaAs quantum dot injection lasers. Appl. Phys. Lett. **69**, 1226–1228 (1996)
6. Y. Wang, V.D. Ta, Y. Gao, T.C. He, R. Chen, E. Mutlugun, H.V. Demir, H.D. Sun, Stimulated Emission and Lasing from CdSe/CdS/ZnS core-multi-shell quantum dots by simultaneous three-photon absorption. Adv. Mater. **26**, 2954–2961 (2014)

7. F. Fan, O. Voznyy, R.P. Sabatini, K.T. Bicanic, M.M. Adachi, J.R. McBride, K.R. Reid, Young-Shin Park, X. Li, A. Jain, Rafael Quintero-Bermudez, M. Saravanapavanantham, M. Liu, M. Korkusinski, P. Hawrylak, V.I. Klimov, S.J. Rosenthal, S. Hoogland, E.H. Sargent, Continuous-wave lasing in colloidal quantum dot solids enabled by facet-selective epitaxy. Nature **544**, 75–79 (2017)
8. A.Y. Liu, J. Peters, X. Huang, D. Jung, J. Norman, M.L. Lee, A.C. Gossard, J.E. Bowers, Electrically pumped continuous-wave 1.3 μm quantum-dot lasers epitaxially grown on on-axis (001) GaP/Si. Opt. Lett. **42**, 338–341 (2017)
9. O.T. Bruns, T.S. Bischof, D.K. Harris, D. Franke, Y. Shi, L. Riedemann, A. Bartelt, F.B. Jaworski, J.A. Carr, C.J. Rowlands, M.W.B. Wilson, O. Chen, H. Wei, G.W. Hwang, D.M. Montana, I. Coropceanu, O.B. Achorn, J. Kloepper, J. Heeren, P.T.C. So, D. Fukumura, K.F. Jensen, R.K. Jain, M.G. Bawendi, Next-generation in vivo optical imaging with short-wave infrared quantum dots. Nat. Biomed. Eng. **1**, 0056 (2017)
10. Chi-Shiang Ke, Chia-Chia Fang, Jia-Ying Yan, J.R. Po-Jung Tseng, Chuan-Pin Chen Pyle, J. Shu-Yi Lin, X.Zhang Chen, Yang-Hsiang Chan, Molecular engineering and design of semiconducting polymer dots with narrow-band, near-infrared emission for in vivo biological imaging. ACS Nano **11**, 3166–3177 (2017). https://doi.org/10.1021/acsnano.7b00215
11. I. Martinić, S.V. Eliseeva, S. Petoud, Near-infrared emitting probes for biological imaging: organic fluorophores, quantum dots, fluorescent proteins, lanthanide(III) complexes and nanomaterials. J. Luminescence **189**, 19–43 (2017)
12. P.O. Anikeeva, J.E. Halpert, M.G. Bawendi, V. Bulović, Quantum dot light-emitting devices with electroluminescence tunable over the entire visible spectrum. Nano Lett. **9**, 2532–2536 (2009). https://doi.org/10.1021/nl9002969
13. K.T. Shimizu, M. Böhmer, D. Estrada, S. Gangwal, S. Grabowski, H. Bechtel, E. Kang, K.J. Vampola, D. Chamberlin, O.B. Shchekin, J. Bhardwaj, Toward commercial realization of quantum dot based white light-emitting diodes for general illumination. Photon. Res. **5**, A1–A6 (2017)
14. G. Zaiats, S. Ikeda, S. Kinge, P.V. Kamat, Quantum dot light-emitting devices: beyond alignment of energy levels. ACS Appl. Mater. Interfaces **9**, 30741–30745 (2017). https://doi.org/10.1021/acsami.7b07893
15. H.C. Yoon, J.H. Oh, S. Lee, J.B. Park, Y.R. Do, Circadian-tunable perovskite quantum dot-based down-converted multi-package white LED with a color fidelity index over 90. Sci. Rep. **7**, 2808 (2017)
16. M.C. Beard, K.P. Knutsen, P. Yu, J.M. Luther, Q. Song, W.K. Metzger, R.J. Ellingson, A.J. Nozik, Multiple exciton generation in colloidal silicon nanocrystals. Nano Lett. **7**, 2506–2512 (2007)
17. V.P. Kamat, Quantum dot solar cells, semiconductor nanocrystals as light harvesters. J. Phys. Chem. C **112**, 18737–18753 (2008)
18. J. Bang, J. Park, J.H. Lee, N. Won, J. Nam, J. Lim, J.B. Park, ZnTe/ZnSe (core/shell) type-II quantum dots: their optical and photovoltaic properties. Chem. Mater. **22**, 233–240 (2009)
19. C.M. Cirloganu, L.A. Padilha, Q. Lin, N.S. Makarov, K.A. Velizhanin, H. Luo, I. Robel, J.M. Pietryga, V.I. Klimov, Enhanced carrier multiplication in engineered quasi-type-II quantum dots. Nat. Commun. **5**, 4148 (2014). https://doi.org/10.1038/ncomms5148
20. S. Tomic, J.M. Miloszewski, E.J. Tyrrell, D.J. Binks, Design of core/shell colloidal quantum dots for MEG solar cells. IEEE J. Photovolt. **6**, 179–184 (2016)
21. M. Liu, O. Voznyy, R. Sabatini, F.P.G. de Arquer, R. Munir, A.H. Balawi, X. Lan, F. Fan, G. Walters, A.R. Kirmani, S. Hoogland, F. Laquai, A. Amassian, E.H. Sargent, Hybrid organic-inorganic inks flatten the energy landscape in colloidal quantum dot solids. Nat. Mater. **16**, 258–263 (2017)
22. B. Sun, O. Voznyy, H. Tan, P. Stadler, M. Liu, G. Walters, A.H. Proppe, M. Liu, J. Fan, T. Zhuang, J. Li, M. Wei, J. Xu, Y. Kim, S. Hoogland, E.H. Sargent, Pseudohalide-exchanged quantum dot solids achieve record quantum efficiency in infrared photovoltaics. Adv. Mater. **29**, 1700749 (2017). https://doi.org/10.1002/adma.201700749
23. A. Franceschetti, H. Fu, L.W. Wang, A. Zunger, Many-body pseudopotential theory of excitons in InP and CdSe quantum dots. Phys. Rev. B **60**, 1819–1829 (1999)
24. M.C. Tamargo, I.L. Kuskovsky, C. Meriles, I.C. Noyan, Enhanced materials based on submonolayer type-II quantum dots (no. DOE-CCNY-0003739-1), Research Foundation of The City College of New York (2017)
25. X. Jin, H. Li, S. Huang, X. Gu, H. Shen, D. Li, X. Zhang, Q. Zhang, F. Li, Q. Li, Bright alloy type-II quantum dots and their application to light-emitting diodes. J. Colloid Interface Sci. **510**, 376–383 (2018). https://doi.org/10.1016/j.jcis.2017.09.080
26. D.J. BenDaniel, C.B. Duke, Space-charge effects on electron tunneling. Phys. Rev. **152**, 683–692 (1966)
27. S.A. Ivanov, M. Achermann, Spectral and dynamic properties of excitons and biexcitons in type-II semiconductor nanocrystals. ACS Nano **4**, 5994–6000 (2010)
28. M. Sahin, F. Koc, A model for the recombination and radiative lifetime of trions and biexcitons in spherically shaped semiconductor nanocrystals. Appl. Phys. Lett. **102**, 183103 (2013)
29. F. Koç, M. Sahin, Electronic and optical properties of single excitons and biexcitons in type-II quantum dot nanocrystals. J. Appl. Phys. **115**, 193701 (2014)
30. F. Koç, K. Koksal, M. Sahin, Effect of a buffer layer between the shell and ligand on the optical properties of an exciton and biexciton in type-II quantum dot nanocrystals. Philos. Mag. **97**, 201–211 (2016). https://doi.org/10.1080/14786435.2016.1252861
31. S. Kim, B. Fisher, H.J. Eisler, M. Bawendi, Type-II Quantum Dots: CdTe/CdSe(Core/Shell) and CdSe/ZnTe(Core/Shell) Heterostructures. J. Am. Chem. Soc. **125**, 11466–11467 (2003)
32. F. Hatami, M. Grundmann, N.N. Ledentsov, F. Heinrichsdorff, R. Heitz, J. Böhrer, D. Bimberg, S.S. Ruvimov, P. Werner, V.M. Ustinov, P.S. Kop'ev, ZhI Alferov, Carrier dynamics in type-II GaSb/GaAs quantum dots. Phys. Rev. B **57**, 4635–4641 (1998)
33. C.M. Tyrakowski, A. Shamirian, C.E. Rowland, H. Shen, A. Das, R.D. Schaller, P.T. Snee, Bright type II quantum dots. Chem. Mater. **27**, 7276–7281 (2015)
34. A. Piryatinski, S.A. Ivanov, S. Tretiak, V.I. Klimov, Effect of quantum and dielectric confinement on the exciton-exciton interaction energy in type II core/shell semiconductor nanocrystals. Nano Lett. **7**, 108–115 (2007). https://doi.org/10.1021/nl0622404
35. E.J. Tyrrell, J.M. Smith, Effective mass modeling of excitons in type-II quantum dot heterostructures. Phys. Rev. B **84**, 165328 (2011)
36. E.J. Tyrrell, S. Tomic, Effect of correlation and dielectric confinement on $1S^{(e)}_{1/2}nS^{(h)}_{3/2}$ excitons in CdTe/CdSe and CdSe/CdTe Type-II quantum dots. J. Phys. Chem. C **119**, 12720–12730 (2015)
37. L.P. Balet, S.A. Ivanov, A. Piryatinski, M. Achermann, V.I. Klimov, Inverted core/shell nanocrystals continuously tunable between type-I and type-II localization regimes. Nano Lett. **4**, 1485–1488 (2004). https://doi.org/10.1021/nl049146c
38. J. Nanda, S.A. Ivanov, H. Htoon, I. Bezel, A. Piryatinski, S. Tretiak, V.I. Klimov, Absorption cross sections and Auger recombination lifetimes in inverted core-shell nanocrystals: implications for lasing performance. J. Appl. Phys. **99**, 034309 (2006). https://doi.org/10.1063/1.2168032
39. J. Nanda, S.A. Ivanov, M. Achermann, I. Bezel, A. Piryatinski, V.I. Klimov, Light Amplification in the Single-Exciton Regime Using Exciton-Exciton Repulsion in Type-II Nanocrystal Quantum Dots. J. Phys. Chem. C **111**, 15382–15390 (2007)

40. K. Matsuda, S.V. Nair, H.E. Ruda, Y. Sugimoto, T. Saiki, K. Yamaguchi, Two-exciton state in GaSb/GaAs type-II quantum dots studied using near-field photoluminescence spectroscopy. Appl. Phys. Lett. **90**, 013101 (2007)
41. Dan Oron, Miri Kazes, Uri Banin, Multiexcitons in type-II colloidal semiconductor quantum dots. Phys. Rev. B **75**, 035330 (2007)
42. V.I. Klimov, S.A. Ivanov, J. Nanda, M. Achermann, I. Bezel, J.A. McGuire, A. Piryatinski, Single-exciton optical gain in semiconductor nanocrystals. Nature **447**, 441–446 (2007)
43. R. Osovsky, D. Cheskis, V. Kloper, A. Sashchiuk, M. Kroner, E. Lifshitz, Continuous-wave pumping of multiexciton bands in the photoluminescence spectrum of a single CdTe-CdSe core-shell colloidal quantum dot. Phys. Rev. Lett. **102**, 197401 (2009)
44. B. Bansal, S. Godefroo, M. Hayne, G. Medeiros-Ribeiro, V.V. Moshchalkov, Extended excitons and compact heliumlike biexcitons in type-II quantum dots. Phys. Rev. B **80**, 205317 (2009)
45. D. Gachet, A. Avidan, I. Pinkas, D. Oron, An upper bound to carrier multiplication efficiency in type II colloidal quantum dots. Nano Lett. **10**, 164–170 (2010). https://doi.org/10.1021/nl903172f
46. H. Zhu, N. Song, T. Lian, Wave function engineering for ultrafast charge separation and slow charge recombination in type II core/shell quantum dots. J. Am. Chem. Soc. **133**, 8762–8771 (2011). https://doi.org/10.1021/ja202752s
47. B. Barman, R. Oszwałdowski, L. Schweidenback, A.H. Russ, J.M. Pientka, Y. Tsai, W.-C. Chou, W.C. Fan, J.R. Murphy, A.N. Cartwright, I.R. Sellers, A.G. Petukhov, I. Žutić, B.D. McCombe, A. Petrou, Time-resolved magnetophotoluminescence studies of magnetic polaron dynamics in type-II quantum dots. Phys. Rev. B **92**, 035430 (2015)
48. Y. Jia, J. Chen, K. Wu, A. Kaledin, D.G. Musaev, Z. Xie, T. Lian, Enhancing photo-reduction quantum efficiency using quasi-type II core/shell quantum dots. Chem. Sci. **7**, 4125–4133 (2016)
49. K. Komolibus, T. Piwonski, C.J. Reyner, B. Liang, G. Huyet, D.L. Huffaker, E.A. Viktorov, J. Houlihan, Absorption dynamics of type-II GaSb/GaAs quantum dots. Opt. Mater. Express **7**, 1424–1430 (2017)
50. P. Klenovský, P. Steindl, D. Geffroy, Excitonic structure and pumping power dependent emission blue-shift of type-II quantum dots. Sci. Rep. **7**, 45568 (2017). https://doi.org/10.1038/srep45568
51. A. Aktürk, M. Sahin, F. Koc, A. Erdinc, A detailed investigation of electronic and optical properties of the exciton, the biexciton and charged excitons in a multi-shell quantum dot nanocrystal. J. Phys. D Appl. Phys. **47**, 285301 (2014)
52. M.A. Leontiadou, E.J. Tyrrell, C.T. Smith, D. Espinobarro-Velazquez, R. Page, P. O'Brien, J. Miloszewski, T. Walsh, D. Binks, S. Tomic, Influence of elevated radiative lifetime on efficiency of CdSe/CdTe Type II colloidal quantum dot based solar cells. Solar Energy Mater. Solar Cells **159**, 657–663 (2017)
53. M. Sahin, S. Nizamoglu, O. Yerli, H.V. Demir, Reordering orbitals of semiconductor multi-shell quantum dot-quantum well heteronanocrystals. J. Appl. Phys. **111**, 023713 (2012)
54. J.P. Perdew, A. Zunger, Self-interaction correction to density-functional approximations for many-electron systems. Phys. Rev. B **23**, 5048–5079 (1981)
55. D.M. Ceperley, B.J. Alder, Ground State of the Electron Gas by a Stochastic Method. Phys. Rev. Lett. **45**, 566–568 (1980)
56. T. Tsuchiya, Biexcitons and charged excitons in quantum dots: a quantum monte carlo study. Phys. E **7**, 470–474 (2000)
57. V.A. Fonoberov, A.A. Balandin, Excitonic properties of strained wurtzite and zinc-blende GaN/AlxGa1-xN/GaN/AlxGa1-xN quantum dots. J. Appl. Phys. **94**, 7178 (2003)
58. M. Gong, W. Zhang, G.C. Guo, L. He, Atomistic pseudopotential theory of optical properties of exciton complexes in InAs/InP quantum dots. Appl. Phys. Lett. **99**, 231106 (2011)
59. P.P. Jha, Philippe Guyot-Sionnest, Trion decay in colloidal quantum dots. ACS Nano **3**, 1011 (2009)
60. G.A. Narvaez, G. Bester, A. Zunger, Excitons, biexcitons, and trions in self-assembled (In, Ga)As/GaAs quantum dots: Recombination energies, polarization, and radiative lifetimes versus dot height. Phys. Rev. B **72**, 245318 (2005)
61. M. Califano, A. Franceschetti, A. Zunger, Lifetime and polarization of the radiative decay of excitons, biexcitons, and trions in CdSe nanocrystal quantum dots. Phys. Rev. B **75**, 115401 (2007)
62. B. Alen, J. Bosch, D. Granados, J. Martinez-Pastor, J.M. Garcia, L. Gonzalez, Oscillator strength reduction induced by external electric fields in self-assembled quantum dots and rings. Phys. Rev. B **75**, 045319 (2007)
63. O. Madelung, *Semiconductors: data handbook* (Springer, Heidelberg, 2004)
64. Su-Huai Wei, S.B. Zhang, A. Zunger, First-principles calculation of band offsets, optical bowings, and defects in CdS, CdSe, CdTe, and their alloys. J. Appl. Phys. **87**, 1304–1311 (2000)
65. C.Y. Chen, C.T. Cheng, C.W. Lai, Y.H. Hu, P.T. Chou, Y.H. Chou, H.T. Chiu, Type-II CdSe/CdTe/ZnTe (core-shell-shell) quantum dots with cascade band edges: the separation of electron (at CdSe) and hole (at ZnTe) by the CdTe layer. Small **1**, 1215–1220 (2005)
66. A.F. Cihan, P.L. Hernandez Martinez, Y. Kelestemur, E. Mutlugun, H.V. Demir, Observation of biexcitons in nanocrystal solids in the presence of photocharging. ACS Nano **7**, 4799–4809 (2013)